JOURNAL OF MATERIALS SCIENCE 31 (1996) 4199–4206

Comparative study of size and distribution of lamellar thicknesses and long periods in polyethylene with a shish-kebab structure

F. ANIA, F.J. BALTÁ CALLEJA
Instituto de Estructura de la Materia,C.S.I.C., c/Serrano 119, E-28006 Madrid, Spain

R.K. BAYER
Institut für Werkstofftechnik, Universität G-H Kassel, Germany

A. TSHMEL
A.F. Ioffe Phys.-Tech. Institute, St. Petersburg, Russia

I. NAUMANN, G.H. MICHLER
Martin-Luther Universität Halle-Wittenberg, Institut für Werkstoffwissenschaft, Geusaer Straße, 06217 Merseburg, Germany

This study contains a combined application of three different techniques for the study of injection moulded polyethylene (PE), showing an oriented shish-kebab structure: small angle X-ray scattering (SAXS), low frequency Raman spectroscopy (LAM) and transmission electron microscopy (TEM). A series of linear PEs and molecular weights in the range 51 000–478 000 has been investigated and two injection temperatures have been used ($T_m = 144$ and 210 °C). SAXS patterns from the highly oriented regions show the presence of either one axial long period (L_1) or two (L_1 and L_2) depending on molecular weight ($\bar{M}_w$) and T_m. It is shown that L_1 and L_2 increase with $\bar{M}_w$ up to a given critical molecular weight $\bar{M}_c$. Above $\bar{M}_c$, L_1 and L_2 remain constant. Raman results qualitatively confirm the existence of two separate distributions of straight-length chain segments for those samples having molecular weights above the critical value. Shorter segments are shown to be more abundant than the longer ones. In the lowest molecular weight sample, results from SAXS, TEM and Raman spectroscopy seem to be consistent with each other, although in some cases a tilted molecular arrangement within the lamellae has to be invoked. On the other hand, in case of the highest molecular weight sample, the length of the short straight-chain segments derived from Raman spectroscopy agrees well with the double periodicity obtained from SAXS. On the contrary, long periods measured from TEM only correspond to the shorter SAXS periodicity. This result is discussed by assuming the occurrence of crystalline bridges among adjacent lamellae.

1. Introduction

It is well known [1–3] that extrusion of polyethylene (PE) above the melting point can give rise to a highly oriented interlocking shish-kebab structure. Such a process is only feasible in a very narrow temperature window, just above the self-blocking temperature of the die, where high wind-up stresses are obtained. In this interval the extruded polymer is largely molten but with a certain concentration of extended chain core crystals which are formed by extensional flow. On cooling, the extended crystals act as nuclei for the epitaxial growth of lamellar crystals with the layer normals along the extrusion direction. Furthermore, lamellae diminish in thickness because the supercooling increases as crystallization proceeds, and interpenetrate with those arising from adjacent extended crystals creating an interlocking platelet assembly. Molecular weight and molecular weight distribution play a very important role in the achievement of the shish-kebab structure [2]. High molecular weight contributes to the formation of the extended-chain fibrils, while low molecular weight components improve extrudability and strength.

Injection moulding as a particular form of extrusion was soon recognized as a potential way for obtaining shish-kebab morphologies [2]. However, conventional moulds mainly provide shear flow in narrow channels and areas close to the cavity walls, and thus do not provide the necessary extensional flow which creates the core crystals. By adequately modifying the geometry of the flow channel a large axial extensional flow component has been successfully introduced into the process [4]. In this way, it has been shown that extensional flow injection moulding (EFIM) of PE is

0022–2461

capable of yielding very similar oriented structures to those obtained by normal extrusion [5]. As compared with conventional injection methods, EFIM yields higher strength materials due to an increase of molecular orientation and the self-reinforcing capability of the shish-kebab fibres [6, 7].

The purpose of the present work is to combine three different, though complementary, techniques: small angle X-ray scattering (SAXS), Raman spectroscopy and transmission electron microscopy (TEM), in order to study the influence that both the molecular weight of a series of linear PE and two different melt temperatures of the EFIM process, play on the morphology and microstructure of the obtained oriented materials. In a discontinuous process such as injection moulding, a minimum molecular weight will still be critical for the formation of extended crystals, but not the low molecular fractions, as the need to support tensile stresses does not arise [2]. In this work, no effort has been made to investigate the influence of the broad molecular weight distribution of the used commercial samples.

2. Experimental procedure

2.1. Materials

A series of commercial linear PEs with average molecular weight in the range $50\,000 < \bar{M}_w < 480\,000$ and molecular weight distributions, $\bar{M}_w/\bar{M}_n$ between 7 and 12, were studied. Elongational flow injection moulded samples with a square cross-section of $4 \times 4\ mm^2$ were prepared for this study. This method provides a high degree of uniaxial orientation in the mouldings [6, 7]. Two different temperatures of the melt were used, $T_m = 144\,°C$ and $T_m = 210\,°C$, while maintaining constant the other processing parameters (injection pressure, mould temperature, etc.). The first T_m value is close to the melting point of the polymer, while the other one is a conventional high-temperature injection temperature. Two different regions from the longitudinal cross-section of the samples were investigated: (1) region I at 0.5 mm from the long axis and (2) region O at 0.5 mm from the outer border (Fig. 1). Both regions are equivalent from the point of view of their measured high birefringence [7], avoiding, respectively, the less oriented central layer (axial flow) and the skin layer where shear flow occurs.

2.2. Techniques

SAXS patterns were obtained at room temperature using a modified Kiessig camera with pinhole collimators of 0.3, 0.5, 0.3 and 0.2 mm diameter, attached to a rotating anode X-ray generator. Ni-filtered CuK_α radiation was employed and the sample–film distance was 500 mm. Sample thickness was approximately equal to 1 mm. Scattered intensity along the meridional direction of the X-ray photographs was obtained by means of a two-beam microdensitometer. The maximum of the scattering peaks was determined after background substraction and the lamellar long spacings were calculated by simple application of Bragg's

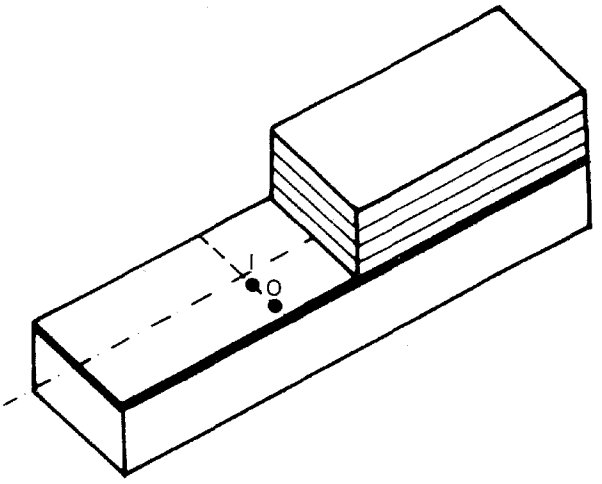

Figure 1 Schematics of an injection moulded sample showing the central layer (black) and the investigated points I and O.

law (no Lorentz correction was performed because of the high orientation of the samples).

The low-frequency Raman transmission spectra were excited by the line at $\lambda = 633$ nm of a 55 mW He–Ne laser and the stray light was analysed in a triple monochromator and converted into electrical pulses in a cooled photomultiplier. The spectra were recorded in 90° geometry in the anti-Stokes range in order to avoid the superposition of He–Ne plasma line at $\approx 15\ cm^{-1}$. For the calculation of the straight-chain segment (SCS) length distribution function, $\mathscr{F}(l)$, the following relation was used [8]

$$\mathscr{F}(l) \propto \left(1 - e^{\frac{-hc\nu}{kT}}\right)\nu^2 I \qquad (1)$$

where c is the speed of light, T is the temperature and I is the scattering intensity at frequency ν. In the case of PE, the SCS length is related to the LAM frequency by the equation

$$\nu_l = \frac{E^{1/2}}{2cl\rho^{1/2}} \qquad (2)$$

where ρ is the density and a value of $E = 370$ GPa was used for the Young's modulus in the chain direction [9].

For electron microscopy, small pyramids were separated from the samples obtaining a cut surface of $0.1 \times 0.1\ mm^2$ at the points I and O, followed by the preparation technique of selective staining by chlorosulphonic acid and osmium tetroxide. $ClSO_3H$ treatment was carried out for 7 days at room temperature, followed by heavy-metal staining during 38 days with a water solution (3%) of osmium tetroxide. The latter is used to enhance the contrast between the crystalline and the amorphous regions. Ultra-thin layers (thickness between 50 and 70 nm) were cut in a cryo-ultramicrotome, then mounted on copper grids and investigated in a 90 kV transmission electron microscope. The thickness, the thickness distribution and the long period of the stacking lamellae were determined by a direct light optical measurement on the electron micrographs.

3. Results

3.1. SAXS long periods

Depending on molecular weight, and to a minor extent on melt temperature, the oriented materials may show either one, L_1, or two, L_1 and L_2, SAXS meridional maxima parallel to the injection direction (Table I). Fig. 2 shows the case of one and two SAXS maxima for a low and a high molecular weight material, respectively. Careful examination of the latter double peak in overexposed films reveals a tendency of the SAXS pattern to be split into a four-point diagram (Fig. 2(b) right). Fig. 3 displays the data measured in the outer region (O) for the two injection melt temperatures $T_m = 144\,°C$ and $T_m = 210\,°C$. Irrespective of injection temperature, it is found that below a certain critical molecular weight, $\bar{M}_c \approx 10^5$, the long periods L_1 and L_2 are proportional to $\bar{M}_x^{1/2}$. An average molecular weight, $\bar{M}_x = 1/2(\bar{M}_w + \bar{M}_n)$, has been defined to minimize the influence of polydispersity on the long period [10]. A similar dependence, only for L_1, has been previously reported in quenched compression moulded PE [11]. Above $\bar{M}_c$, L_1 and L_2 remain nearly constant with increasing $\bar{M}_x$, showing values close to 30 and 55 nm respectively (Table I). The critical molecular weight for the appearance of the second long spacing (L_2) coincides with $\bar{M}_c$ for those samples injected at high melt temperature (210 °C) and it is lower for $T_m = 144\,°C$. The critical molecular weight, $\bar{M}_c$, has been associated to a percolation process of a network of stable entanglements, which leads to a drastic improvement in the mechanical properties of the material [7]. Similar results have been observed in the long periods measured in the inner region (I), but with some differences which will be outlined below.

As a general rule, the long period values measured in region I are always higher that the corresponding ones in the outer part O. Fig. 4 shows the difference between the corresponding L_1 values for all the investigated samples. The positive difference $\Delta L_1 = L_1(I) - L_1(O)$ is influenced by the slower cooling rate which takes place in the inner regions, favouring the growth of larger crystallites. Taking a closer look it is noteworthy that, for the high injection melt temperature, ΔL_1 shows a constant value of ~ 4 nm, except for the low molecular weight materials where it increases continuously up to a value of ~ 9 nm. On the other hand, for the low melt temperature, ΔL_1 is close to zero below $\bar{M}_c$ and shows again a constant value of

TABLE I SAXS long spacings [nm] of the PE injection moulded materials

$\bar{M}_w \times 10^{-3}$	$T_m = 210\,°C$				$T_m = 144\,°C$			
	I		O		I		O	
	L_1	L_2	L_1	L_2	L_1	L_2	L_1	L_2
51	23		22		30		21	
58	24		23		31		24	
71	25		23		28		24	
80	26		26		31	49	27	46
108	28		28		31	55	27	49
182	33	56	28	53	33	55	30	55
190	34	60	31	57	34	62	30	58
478	35	56	32	55	35	62	31	56

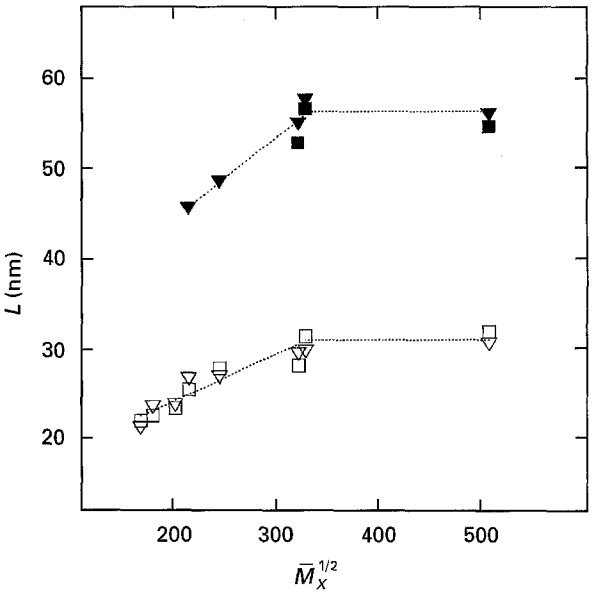

Figure 3 SAXS long spacings as a function of $\bar{M}_x^{1/2}$ measured in region O for the two injection melt temperatures: $T_m = 144\,°C$ (▽) and $T_m = 210\,°C$ (□). Solid symbols correspond to L_2 and open symbols to L_1.

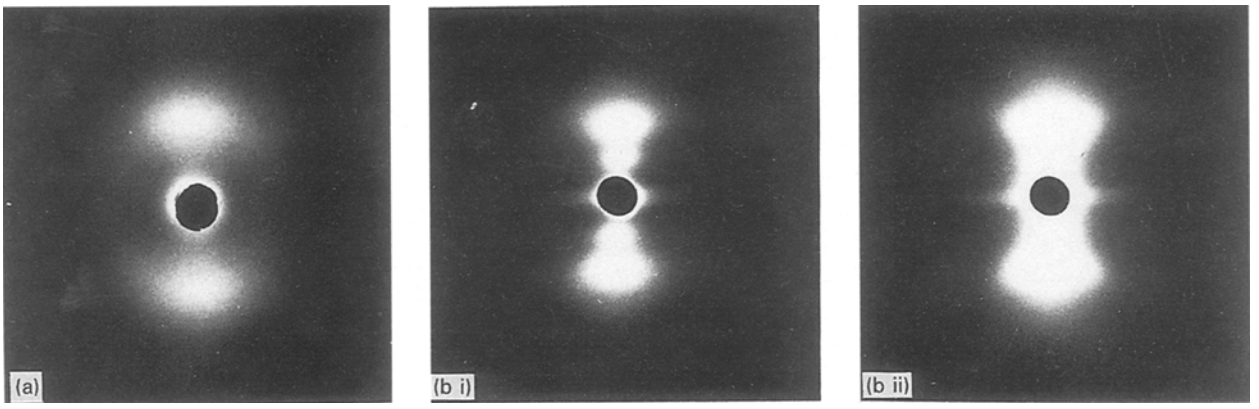

Figure 2 SAXS patterns of two samples with molecular weight: (a) $\bar{M}_w = 58 \times 10^3$ and (b) $\bar{M}_w = 182 \times 10^3$ (two different exposure times: 3 h and 24 h).

~4 nm for higher molecular weights. Considering now the difference $\Delta L_1^* = L_1(144\,°C) - L_1(210\,°C)$, is observed to be negligible in the outer region O, while in the inner region it is a decreasing function of the molecular weight below $\bar{M}_c$, becoming zero above this point (Fig. 5). These effects ought to be dependent on the network of physical entanglements of the melt,which is partly transferred into the solid state during the injection process. Such a network only exists above a critical molecular weight and has been proved to be better developed for higher molecular weights and lower melt temperatures [7].

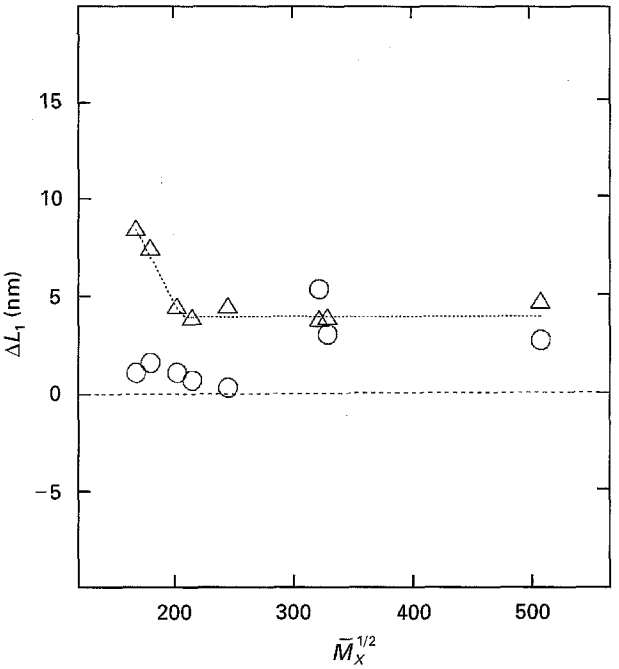

Figure 4 Plot of the difference, $\Delta L_1 = L_1(I) - L_1(O)$, in SAXS long spacing between regions I and O, as a function of $\bar{M}_x^{1/2}$. (Δ: $T_m = 144\,°C$, ○: $T_m = 210\,°C$).

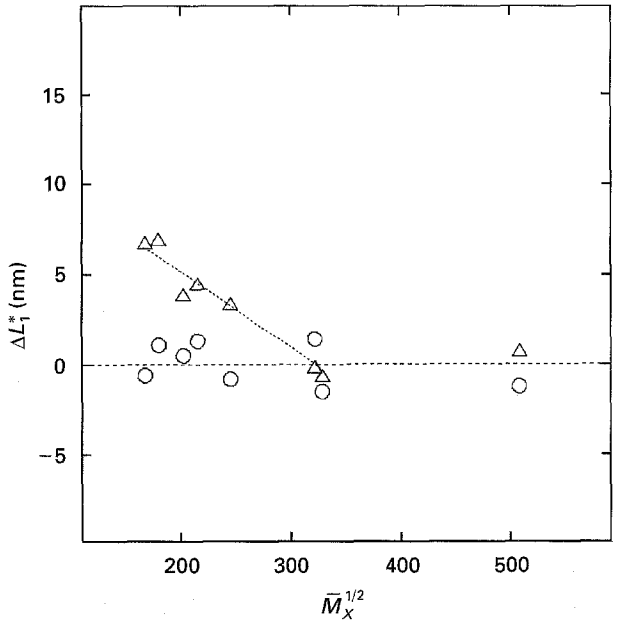

Figure 5 Plot of the difference, ΔL_1^*, in SAXS long spacing L_1 for the two injection melt temperatures, 144 and 210 °C, as a function of $\bar{M}_x^{1/2}$. (Δ: region I, ○: region O).

3.2. Raman SCS lengths

A very similar qualitative picture is obtained from low frequency Raman spectroscopy data of the low melt temperature series ($T_m = 144\,°C$). It is found that a unique LAM band with the maximum located at 16–17 cm^{-1} appears for those samples with average molecular weight between 51×10^3 and 71×10^3. The band position shifts to lower frequency with increasing molecular weight. When $\bar{M}_w$ reaches 182×10^3, the uprising of an extra LAM mode starts from the low frequency tail of the previous one. On further increasing $\bar{M}_w$ the frequency of both LAM modes continues to decrease, and the spectrum for the sample with the highest molecular weight shows two well-resolved peaks at 12.5 and 9.5 cm^{-1} in the outer layer and at 12 and 8 cm^{-1} in the inner region. The calculated and normalized straight-length distribution functions, $\mathcal{F}(l)$, are shown in Fig. 6. The position of their peak maxima refers to the average SCS length within crystallites. These results are collected in Table II and are also represented in Fig. 7 as a function of molecular weight. In addition, the bimodal distributions have been empirically separated into two components. The area ratio $A_1/(A_1 + A_2)$ between the two separate populations represents the relative proportion of long SCS segments [9]. The variation of this ratio indicates that, in all cases, long SCS segments are less abundant than the shorter ones, increasing in relative number with increasing molecular weight (see Table II).

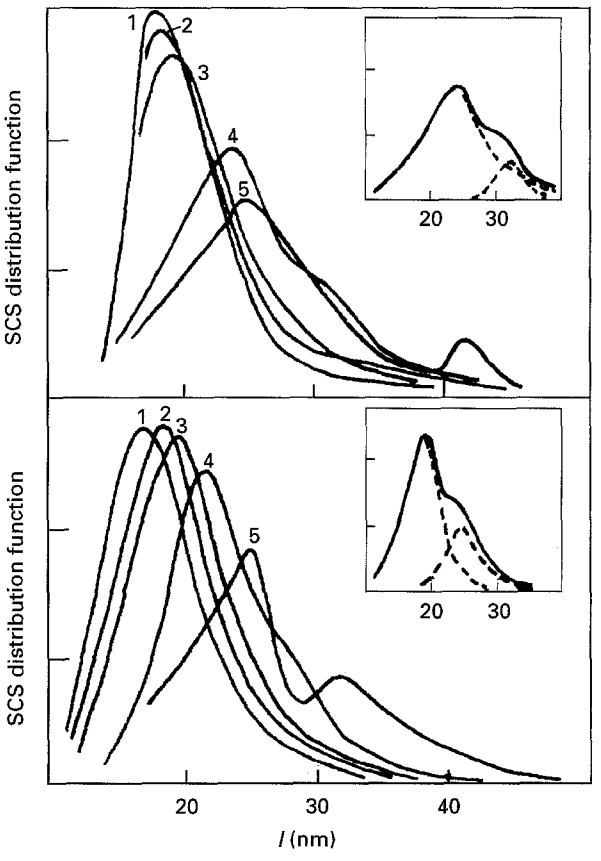

Figure 6 Straight-chain segment (SCS) length distribution function, from LAM, for different molecular weights ($\times 10^{-3}$): (1) 51, (2) 58, (3) 71, (4) 182, (5) 478, Insert: 190. Upper figure: region I. Lower figure: region O.

TABLE II Raman average straight-chain segment lengths [nm] and area ratio, $A_1/(A_1 + A_2)$, of the resolved distribution functions

$M_w \times 10^{-3}$	$T_m = 144\,°C$					
	I			O		
	l_1	l_2	$\frac{A_1}{A_1 + A_2}$	l_1	l_2	$\frac{A}{A_1 + A_2}$
51	18			16.5		
58	19			17.5		
71	18			19		
182	24	30	0.12	21	27	0.07
190	25	33	0.14	19.5	28	0.28
478	25	40	0.16	25	32	0.29

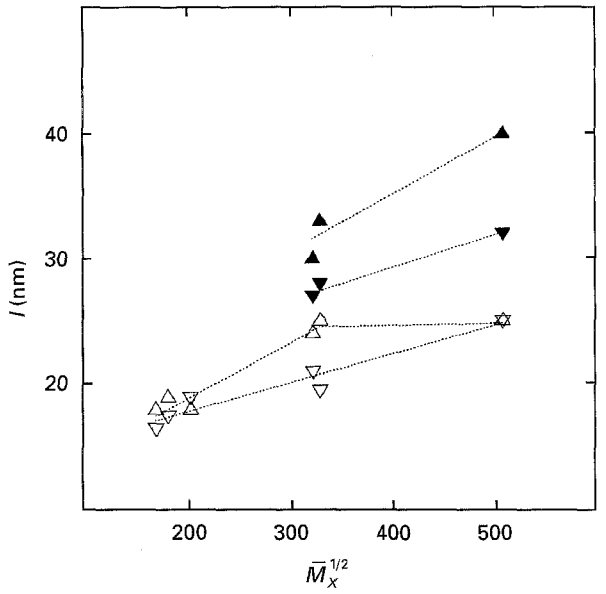

Figure 7 LAM SCS length as a function of $\bar{M}_x^{1/2}$ for $T_m = 144\,°C$. (Δ: region I, ∇: region O). Solid symbols correspond to l_2 and open symbols to l_1.

3.3. Electron microscopy

For the electron microscopy study, two samples corresponding to the lowest molecular weight (51×10^3) and the highest one (478×10^3) were chosen. For both, the temperature of the melt was 144 °C.

The low molecular weight material shows, in the inner region, stacks of lamellae which are locally arranged in a, more or less, random manner (Fig. 8(a)). The arrangement of lamellae occurs in bundles which, in some areas, are perpendicular to the injection direction (Fig. 8(b)) giving rise to a local orientation. The thickness D_i of lamellae (internal lamellar thickness = crystalline part inside the lamellae) varies between 3 and 14 nm with an average value of 8.5 nm. The frequency distribution of lamellar thicknesses is shown in Fig. 9. In the outer region, a similar picture is found with the exception of a surface layer, < 100 μm thick, where a completely different morphology appears. Here, a microfibrillar structure, with thick microfibrils nearly parallel to the injection direction, is observed (Fig. 10). The microfibrils are considerably thicker than the lamellae, ranging from 10 to 140 nm, and a maximum in the thickness frequency distribution of about 30 nm (Fig. 11).

The high molecular weight material shows in the outer region a well defined orientation of lamellae belonging to a conspicuous shish-kebab structure (Fig. 12). Lamellae, sharply limited to the amorphous regions, are arranged in bands (shish-kebabs) with shish fibril widths of a few tenths of micrometres and lengths of several micrometres. Lamellar thicknesses vary between 4 and 15 nm, with an average value of about 9 nm (Fig. 13).

In addition to the lamellar thicknesses, the long periods from the shish-kebab lamellar stacks were also directly determined on the micrographs. Values between 13 and 31 nm were obtained. The frequency distribution of the long period has only in some places a bimodal shape (Fig. 14).

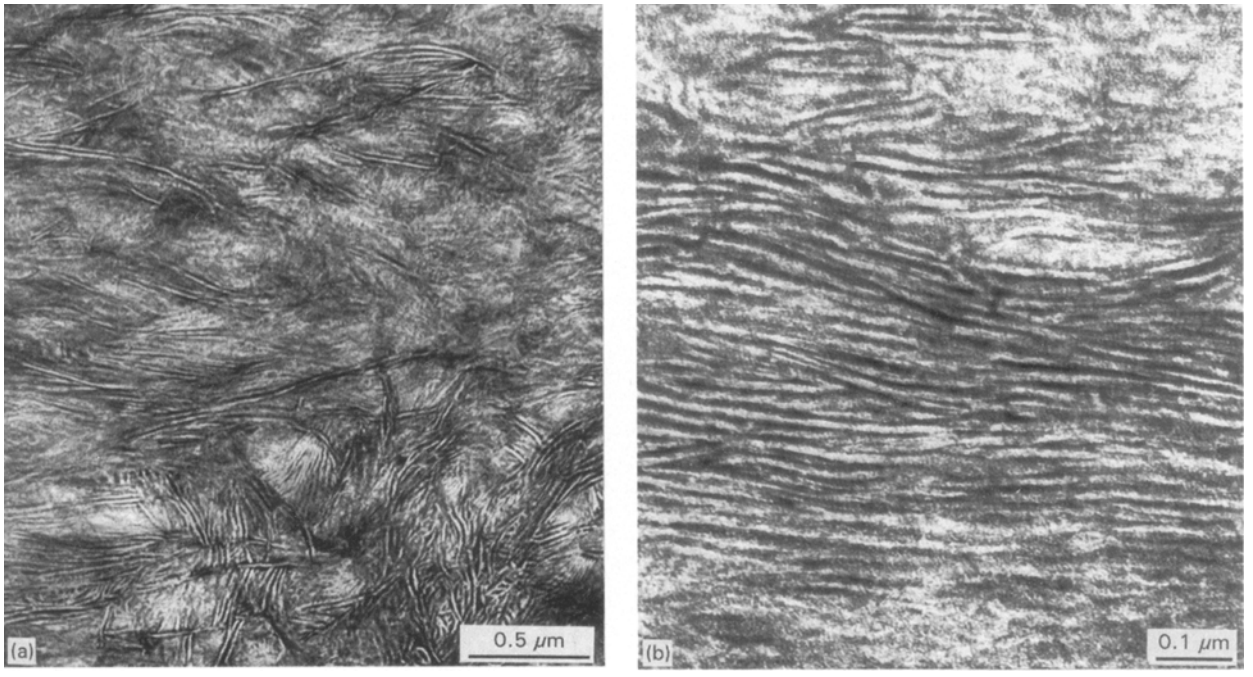

Figure 8 Micrographs of two different details within the region I of a low molecular weight material ($\bar{M}_w = 51 \times 10^3$).

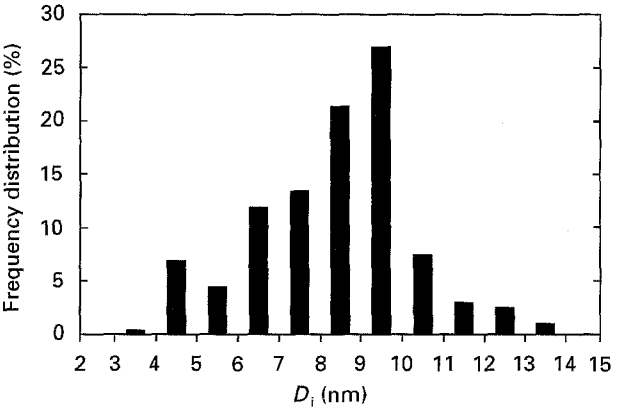

Figure 9 Frequency distribution of lamellar thickness, D_i, of the same material as in Fig. 8.

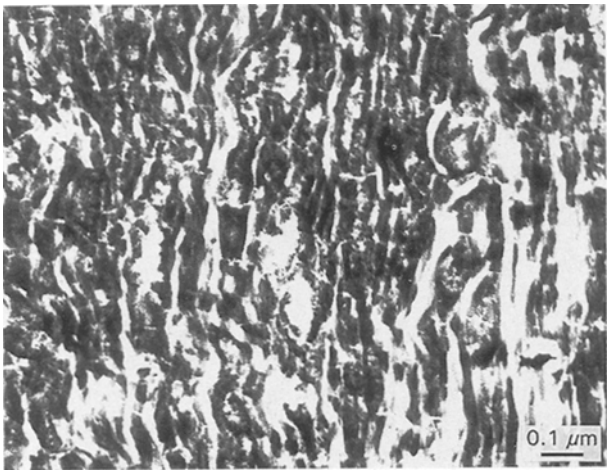

Figure 10 Micrograph from region O of the same material as in Fig. 8.

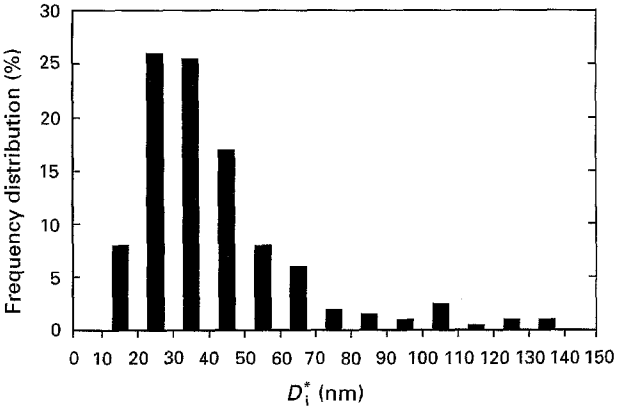

Figure 11 Frequency distribution of microfibrillar thickness, D_i^*, of the same region and material as in Fig. 10.

In the inner region a well pronounced parallel arrangement of lamellae forming shish-kebab structures can be observed, but in some areas also a weaker and not clear orientation has been detected.

4. Discussion

Comparison of the techniques of SAXS, Raman spectroscopy and electron microscopy has been undertaken before examining particular details of the

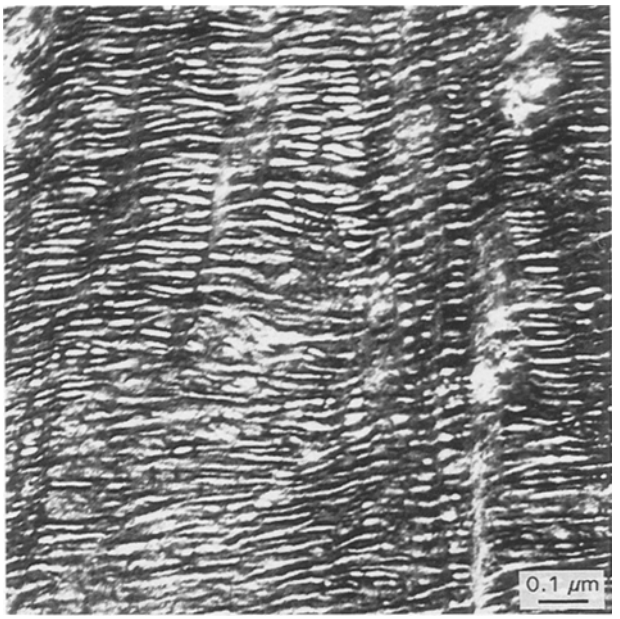

Figure 12 Micrograph from region O of a high molecular weight material ($\bar{M}_w = 478 \times 10^3$).

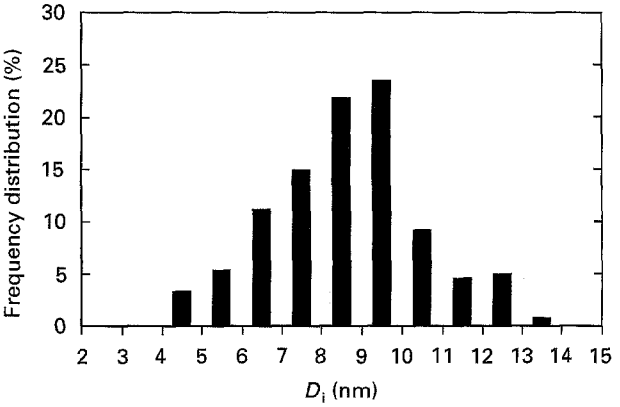

Figure 13 Frequency distribution of lamellar thickness, D_i, of the material as in Fig. 12.

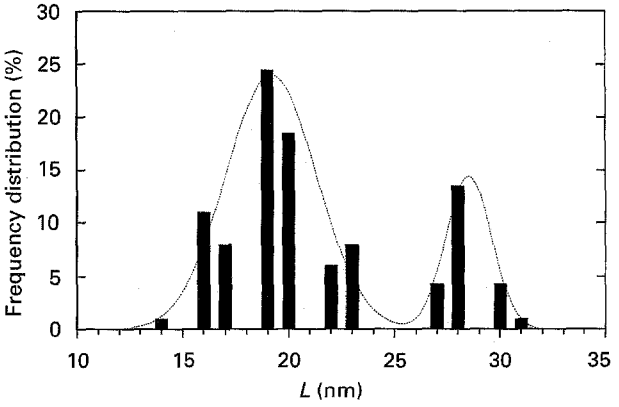

Figure 14 Frequency distribution of long periods, L, of the material as in Fig. 12, showing a bimodal shape.

microstructure of PE (see for example [12]). In the present work, we intend to make use of the above techniques to review some still controversial aspects of the shish-kebab morphology. In this respect it is important to fully understand which is the information

provided by each particular technique and which are their limitations.

The appearance of a SAXS maximum is commonly associated to a periodical fluctuation of electron density along a certain direction. Assuming the most simple two-phase model, such a fluctuation corresponds to a regular stacking of crystalline lamellae and amorphous regions. The existence of a second SAXS maximum, L_2, could be originated by a different lamellar periodicity, or it could be related to a second order of the first stacking periodicity. It is, therefore, important to elucidate whether L_1 and L_2 are mutually related. For all the investigated high molecular weight samples, the L_2/L_1 ratio yields an average value of 1.76, a result that does not rule out the possibility of both long periods being different orders of the same repeating structure. However, SAXS [13] and recent USAXS [14] experiments as a function of temperature have given conclusive evidence that the two periodicities are independent of each other. It is observed that, on heating, the lower spacing shifts towards lower scattering angles, till it merges with the L_2 peak, which meanwhile remains unchanged. From this point, up to the vicinity of the melting point, the single long period increases again. On cooling, after having melted the material, two new long periods appear whose values depend on thermal history. The existence of a double long period at room temperature has been recently associated to a shish-kebab fibrillar structure arising during the elongational flow injection process [15]. During this process, it is reasonable to admit the appearance first of dominant lamellae, while the space between them is later filled by thinner subsidiary crystalline structures in the form of lamellae [14], crystal blocks or crystalline bridges. Two long periods in PE have also been found by shear induced crystallization [16] and in melt crystallized high molecular weight materials [12]. The tendency of the SAXS maxima to split and form a certain angle ($\beta \sim 18°$) with the meridional direction (Fig. 2(b)), suggests that the lamellar basal planes form in the average the above mentioned angle with the injection direction. This result is in accordance with previous TEM observations [17] and with our present micrographs.

LAM spectra yield straight chain segment lengths which are related to the internal lamellar thickness. If these segments were perpendicular to the basal planes, the difference between the L values derived from SAXS and the l results obtained from LAM should offer an estimate of the thickness of the amorphous interlamellar layer including the boundary interphase. By comparing the results of Tables I and II it is seen that the difference between $L_1\cos\beta$ (SAXS) and l_1 (LAM) does not change significantly for all investigated samples showing an average value of 7 ± 2 nm. Similarly, $L_2\cos\beta$ (SAXS) $- l_2$ (LAM) takes a constant average value of 24 ± 3 nm. The ratio $l/(L\cos\beta)$ should yield a rough approximation to the linear degree of crystallinity of the material. This ratio is about 0.8 and 0.6, for the shorter and longer spacings, respectively. At this point one should take into consideration the nature of the LAM Raman bands. It is known that the region of LAM localization is restricted by the regular trans-zigzag periodicity [9]. Usually, chain defects are located at the interphase between crystalline regions [18], but also a significant number of conformational defects may exist inside a crystal [19]. Such defects are undetectable by SAXS, but could drastically reduce the size of l(LAM) giving as a result a much lower $l/(L\cos\beta)$ ratio. On the contrary, the presence of a certain tilt of the SCS molecular segments with respect to the lamellar basal planes would increase the $l/(L\cos\beta)$ value in relation to the linear crystallinity.

Concerning TEM observations, for the lowest molecular weight material investigated, the appearance of a microfibrillar structure near the surface is quite surprising. It indicates a high molecular orientation which is in good agreement with previous birefringence results [7]. TEM lamellar thicknesses can be translated into long period values according to the expression [20, 21]

$$L = D_i + 2g + D_a \tag{3}$$

where the long period L contains the internal lamellar thickness D_i, the two g thicknesses of both boundary layers and the thickness D_a of the amorphous interlamellar layer. By assuming $g = 2$ nm and $D_a \approx D_i$ [20, 21], lamellar thicknesses of 4–13 nm would yield long periods between 12 and 30 nm. The average of the latter L (TEM) values coincides with the SAXS result (see Table III). On the other hand, the length of extended chain crystals derived from Raman spectroscopy is about 17 nm. To correlate this value, with the thickest observed lamellae of $D_i = 13$ nm, a tilted arrangement of the stretched molecular segments inside lamellae must be invoked. This inclined molecular arrangement would result in a maximum tilt angle of 38° of the SCS segments with respect to the lamellar basal planes [22].

For the high molecular weight material, there is a clearly pronounced lamellar orientation in the form of a shish-kebab structure. The long periods directly measured on micrographs vary between 13 and 31 nm.

TABLE III Comparison of results, from the outer region O, for the two extreme molecular weights: LMW = 51×10^3 and HMW = 478×10^3, for $T_m = 144$ °C

	Long period			Crystal thickness		
	L (SAXS)		L (TEM)	l (Raman)		D_i (TEM)
LMW	21		12–30	16.5		4–13
HMW	31	56	13–31[a]	25	32	4–15

[a] Direct determination: sometimes bimodal.

At the same time, the evaluation of lamellar thicknesses on the same micrographs yields an interval of 4–15 nm, which according to Equation 3 represents long period values of 12–34 nm, very close to the experimental ones. Therefore, it seems that long periods measured by TEM only correspond to the shorter SAXS periodicity (Table III). In addition, TEM observations show, in most cases, just a smaller variation of the lamellar thicknesses around a single distribution. These different results can be explained if one admits the existence of a large contribution of tie taut molecules or crystalline bridges between adjacent lamellae which contribute to the larger Raman peak and to the higher X-ray long periods. Such regions are probably not well defined by the selective staining used for TEM, and neglected for long spacing determination, because measurements are only carried out in those regions where sharp interlamellar regions are observed. In this way TEM long periods can be effectively correlated to the shorter spacings.

5. Conclusions

Small angle X-ray scattering of these oriented materials confirms the presence of one or two independent meridional maxima, depending on molecular weight and melt temperature. The corresponding long periods increase with molecular weight upto a critical molecular weight, remaining constant for higher values of $\bar{M}_w$. The critical molecular weight has been associated, in a previous work [7], to a percolation process of a network of physical entanglements.

Raman spectroscopy data qualitatively confirm the existence of two separate distributions of straight-length chain segments for those samples having molecular weights above the critical value. Shorter segments are shown to be more abundant than the longer ones.

Electron microscopy, in turn, shows a rich variety of morphologies which corresponds to the non-homogeneous nature of the investigated samples. The low molecular weight material shows a 100 μm surface skin layer containing a microfibrillar structure with a high molecular orientation. The rest of the material presents different arrangements of lamellae in the form of bundles, which in local areas, show a small global orientation. The high molecular weight material shows mainly a shish-kebab structure, which is better defined in the outer region.

The combination of SAXS, Raman spectroscopy and TEM draws a qualitative picture for the low molecular weight material, as having a single distribution of lamellar crystal thicknesses with molecular chains forming a certain angle with its basal planes. The high molecular weight samples show, on the other hand, the presence of two different populations of crystal thicknesses. However, TEM observations yield only information about the shorter periodicity. The occurrence of a certain fraction of tie taut molecules and crystalline blocks between adjacent lamellae has been suggested to explain the latter result.

Acknowledgements

Grateful acknowledgements is due to DIGICYT, Spain (Grant PB94-0049) and DAAD, Germany and DIGICYT (Grant HA94-193B) for the support of this investigation.

References

1. J. A. ODELL, D. T. GRUBB and A. KELLER, *Polymer* **19** (1978) 617.
2. Z. BASHIR, J. A. ODELL and A. KELLER, *J. Mater. Sci.* **19** (1984) 3713.
3. *Idem., Ibid.* **21** (1986) 3993.
4. R. K. BAYER, Conference Abstracts 14th Europhysics Conference on Macromolecular Physics, Vilafranca del Penedès (Spain) **69** (1982) 75.
5. W. HECKMANN, Ph.D. Thesis, TH Darmstadt (1976).
6. R. K. BAYER, A. E. ELIA and J. C. SEFERIS, *Polym. Eng. Rev.* **4** (1984) 201.
7. R. K. BAYER. F. J. BALTÁ CALLEJA, E. LOPEZ CABARCOS, H. G. ZACHMANN, A. PAULSEN, F. BRÜNING and W. MEINS, *J. Mater. Sci.* **24** (1989) 2643.
8. R. G. SNYDER, S. J. KRAUSE and J. R. SCHERER, *J. Polym. Sci., Polym. Phys. Ed.* **16** (1978) 1593.
9. A. TSHMEL, I. A. GORSHKOVA and V. M. ZOLOTAREV, *J. Macromol. Sci. Phys.* **B32** (1993) 1.
10. E.S. HSIUE, R. E. ROBERTSON and G. S. Y. YEH, *Ibid.* **B22** (1983) 305.
11. J. RAULT, *CRC Crit. Rev. Solid State and Mater. Sci.* **13** (1986) 57.
12. J. DLUGOSZ, G. V. FRASER, A. KELLER, J. A. ODELL and P. L. GOGGIN, *Polymer* **17** (1976) 471.
13. J. MARTINEZ-SALAZAR, J. V. GARCIA RAMOS and J. PETERMANN, *Intern. J. Polymeric Mater.* **21** (1993) 111.
14. D. R. RUEDA, F. ANIA and F. J. BALTÁ CALLEJA, *Polymer* (submitted).
15. F. ANIA, R. K. BAYER and F. J. BALTÁ CALLEJA, *Ibid.* **33** (1992) 233.
16. G. S. Y. YEH, *Rubber Chem. Technol.* **50** (1977) 863.
17. Z. BASHIR, M. J. HILL and A. KELLER, *J. Mater. Sci. Lett.* **5** (1986) 876.
18. H. G. KILIAN, *Colloid Polym. Sci.* **262** (1984) 374.
19. F. J. BALTA CALLEJA, in "Morphology of polymers", edited by B. Sedláček (Walter de Gruyter & Co., Berlin, 1986) p. 27.
20. G. H. MICHLER and I. NAUMANN, *Acta Polymerica* **33** (1982) 399.
21. G. H. MICHLER and E. BRAUER, *Ibid.* **34** (1983) 533.
22. G. H. MICHLER and I. NAUMANN, in "Morphology of polymers", edited by B. Sedláček (Walter de Gruyter & Co., Berlin, 1986) p. 329.

Received 18 December 1995
and accepted 13 February 1996